Ab initio molecular-dynamics study of liquid $GeSe_2$

Mark Cobb and D. A. Drabold
Department of Physics and Astronomy, Condensed Matter and Surface Sciences Program, Ohio University, Athens, Ohio 45701-2979
(Received 29 January 1997)

The structural, vibrational, and electronic properties of liquid $GeSe_2$ are investigated using *ab initio* molecular dynamics. The static structure factor $S(Q)$ and the pair-correlation functions of our model are in good agreement with experiment. We find many similarities between the topology of the liquid and the glass state. In addition we introduce a way of characterizing the intermediate-range order of liquid and glassy $GeSe_2$ through fourfold and sixfold rings. The overall vibrational density of states is found to be consistent with Raman experiments. The intensity of the low-frequency modes, splitting of the A_1 and A_{1c} peaks, and the decrease in the intensity of the high-frequency modes are all reproduced. The electronic density of states is determined and compared to our results for glassy $GeSe_2$. We find that an increase in Se bond length and bond-angle disorder significantly broadens the conduction band. The time-dependent behavior of the electronic eigenvalues is examined and transient events are observed in which an electronic state crosses the optical gap. The structural configurations which produce states in the optical gap are determined using an *ab initio* molecular-dynamics approach and are found to be in agreement with experimental photoluminescence and electron-spin-resonance data. We also find that a linear relationship exists between the root mean square of the thermal fluctuations of an electronic eigenvalue in time and its localization. [S0163-1829(97)05830-X]

I. INTRODUCTION

The ability of a material to form a glass when it is supercooled from the liquid state is still not well understood. In order to understand the glass-forming ability of a material it is essential that the topology of its liquid state be determined. The chalcogens (S,Se,Te) and chalcogenide alloys are well-known glass-forming materials and their structural properties have been studied extensively in the glass and liquid states. Structural information pertaining to the liquid and glass is limited to the experimental static structure factor (and thus the total and partial pair-correlation functions). Because of these experimental limitations it becomes necessary to construct models to obtain more information about the liquid and glass states. In the last decade *ab initio* molecular dynamics has become the most sophisticated approach for the study of disordered materials and liquids.

In this paper we present results of an *ab initio* molecular-dynamics study of liquid $GeSe_2$ (l-$GeSe_2$). It is a covalently bonded semiconductor which is largely composed of linked $Ge(Se_{1/2})_4$ tetrahedra. In our previous papers (Refs. 1,2) we examined the structural, vibrational, and electronic properties of g-$GeSe_2$ in detail. Our earlier work demonstrated that the time scales of an *ab initio* calculation, although orders of magnitude shorter than experiment, were long enough to generate the correct chemistry and topology of g-$GeSe_2$ through a process of simulated annealing and quenching. This suggests that the liquid state (from which the g-$GeSe_2$ model was created) should have the correct average chemistry and topology. The main topics of this paper are the structural, vibrational, and electronic properties of l-$GeSe_2$. Because the liquid is not a static structure we average over many time steps to obtain a more accurate description of its properties. To obtain this information we perform microcanonical molecular dynamics on the equilibrated liquid near 1000 K over 1.0 and 3.5 ps with a time step of 3.5 fs. This temperature is near the melting point of crystalline $GeSe_2$ and it is also the temperature at which the liquid is quenched to form the glass. Determining the structural properties of the liquid at this temperature provides crucial information about how the topology of the liquid, glass, and high-temperature crystal phase are related.

The structure of l-$GeSe_2$ is determined through the static structure factor $S(Q)$, partial pair-correlation functions, angle distribution functions, and ring structures. The static structure factor can be compared directly to experiment and we find that our model's total $S(Q)$ is in good agreement with experimental neutron scattering results of Refs. 3,4. A different study by Penfold and Salmon (Ref. 5) has characterized the neutron-scattering partial static structure factors and the real-space partial pair-correlation functions. We find good agreement with their partial structure factors and partial pair-correlation functions. An important use of our *ab initio* l-$GeSe_2$ and g-$GeSe_2$ models is the determination of angle distributions. Angle distributions provide information essential to the interpretation and analysis of experimental data (Ref. 5).

One of the remarkable features of g-$GeSe_2$ is the first sharp diffraction peak (FSDP) of its $S(Q)$ around 1.0 $Å^{-1}$. The FSDP is a clear indication of intermediate range order (IRO) on a length scale of approximately 6.0 Å. The $S(Q)$ of l-$GeSe_2$ has an FSDP as well which suggests that there is intermediate-range structural order in the liquid before the crystal or glass state is reached. Because the crystal phase naturally emerges from the liquid state with cooling one might expect that the IRO of the liquid is similar to the IRO of the crystal. This would also suggest that the IRO of the glass is related to the IRO of the crystal as well. The high-temperature crystal phase of $GeSe_2$ is formed from two-dimensional layers and these layers are know to be chemically ordered and composed of fourfold and sixfold rings. It might be expected then that g-$GeSe_2$ would have to some

extent an ordering of fourfold and sixfold rings similar to that of the crystal. An important goal of this paper is to provide a more fundamental characterization of the IRO in l-$GeSe_2$ and g-$GeSe_2$ in terms of the correlations between the fourfold and the sixfold rings in these materials.

We introduce a set of correlation functions which involve correlations between fourfold and sixfold rings. The center of mass (CM) of the fourfold and sixfold rings are determined and this information is used to calculate partial static structure factors for a network of fourfold and sixfold ring CM's. In both the liquid and the glass we find that all of these rings $S(Q)$ display a very strong peak around 1.0 $Å^{-1}$ indicating that they have intermediate-range order correlations of about 6 Å. In addition we also calculate the total $S(Q)$ of the glass with the correlations between fourfold (4-4), sixfold (6-6), and fourfold and sixfold rings (4-6) within a range of 4.6–9.0 Å eliminated. We find that this procedure removes the FSDP from the glass $S(Q)$. From these results we are able to characterize the IRO of liquid and glassy $GeSe_2$ in a different and more fundamental way than previous attempts (Refs. 6,7).

Liquid $GeSe_2$'s vibrational density of states (VDOS) has been inferred from experimental Raman-scattering measurements (Ref. 8). A direct comparison between our results for the VDOS and those of Ref. 8 is not possible (because they measure the VDOS indirectly through the optical properties of the liquid) and inelastic neutron-scattering measurements have not been made on l-$GeSe_2$. Instead we focus on the qualitative peak structure and the differences between the glass and liquid VDOS. We find that our model reproduces the three major bands of the Raman measurements. The splitting of the A_1 and A_{1c} peaks and their relative intensities are reproduced. Our results also agree with those of experiment which indicate that the intensity of the high-frequency band is much less intense in the liquid than it is in the glass.

The last section of this paper will focus on the electronic structure of the liquid. We find that the electronic density of states (EDOS) of l-$GeSe_2$ is quite similar to that of g-$GeSe_2$. The most significant difference between the liquid and the glass EDOS is that the conduction band of the liquid extends much further into the optical gap. We find that the conduction band broadening can be attributed to the local network topology. The average localization of the electronic states is determined as well. From annealing the liquid near 1000 K we observe that the root mean square (rms) of the thermal fluctuation of an electronic eigenvalue in time is essentially a linear function of its charge localization (Ref. 9).

The time evolution of the electronic eigenvalues is examined and states are observed moving across the optical gap. We find that these states result from the formation of valence- and conduction-band configurations on atoms with a large degree of electronic localization. Electronic states in the optical gap of the glass have been detected through light-induced electron-spin-resonance (LESR) and photoluminescence measurements (Refs. 10,11) and they appear to be associated with Ge and Se coordination defects. From the experimental data we infer the basic characteristics of the Ge and Se defect states and compare them to the states crossing the optical gap of our liquid model.

II. MODEL

Computations described in this section were performed using the *ab initio*, local basis density-functional method of Sankey and co-workers.[12] The essential approximations are (1) Bachelet-Hamann-Schlüter pseudopotentials,[13] (2) the Harris functional,[14] (3) the local-density approximation,[15] and (4) a minimal basis set of one s and three p confined pseudoatomic orbitals per site. The method has met with great success in a wide variety of systems, and provides a transferable description of covalently bonded materials. In addition, application of a self-consistent variant of this Hamiltonian to our glass model of $GeSe_2$ (Ref. 2) produced similar results.[16]

A cubic supercell 18.76 Å on a side with 144 selenium atoms and 72 germanium atoms placed on a diamond lattice was chosen for the initial configuration of our model. This gave our model the correct stoichiometry and by construction a number density close to the experimental one of 3.116×10^{22} cm^{-3} (see Ref. 3). The initial temperature of the cell was 6000 K, it was then equilibrated to 5000 K over approximately 600 fs. The cell was then cooled to 1000 K and equilibrated at this temperature for approximately 1 ps. We then generated 1.0 and 3.5 ps long trajectories by performing microcanonical molecular dynamics with a time step of 3.5 fs. The long time step of 3.5 fs is suitable for the heavy atoms of our system (Ge is 72.59 a.m.u. and Se is 78.96 a.m.u.) and does not cause problems with energy conservation. Because the simulations were microcanonical the temperature fluctuated. The average temperature of these simulations was 1117 and 1144 K with standard deviations of 49 and 51 K, respectively. All of our calculations were done using only the Γ point to sample the Brillouin zone. The Γ point is a suitable choice because of the small size of the Brillouin zone.

III. STRUCTURAL PROPERTIES

A. Static structure factor

The total and partial structure factors are defined as in Ref. 2 and the Ge and Se scattering lengths are 0.819 and 0.797, respectively, in units of 10^{-4} Å. The total static structure factor (Fig. 1) is in excellent agreement with the results of various neutron-scattering experiments (Refs. 3,4). This is an improvement over our model of g-$GeSe_2$ in which the second peak was weaker then the experimental neutron-scattering results of Ref. 3. In our study of the glass we determined that the high degree of chemical disorder in our model could be attributed to the short quenching time scales of the calculation. The effects of short-time scales will be less important in our liquid model. We therefore expect better agreement between theory and experiment in the case of the liquid. A direct comparison can be made with the partial $S_{\alpha\beta}(Q)$'s (Fig. 2) determined from neutron scattering results in Ref. 5. Our $S_{\alpha\beta}(Q)$'s are in qualitative agreement with the results of Ref. 5 but the relative intensities are quite different. Because our partial $S_{\alpha\beta}(Q)$'s can be summed to obtain the total $S(Q)$ we believe that the discrepancy between our results and those of Ref. 5 is due to the manner in which the partial $S(Q)$'s are defined in Ref. 5.

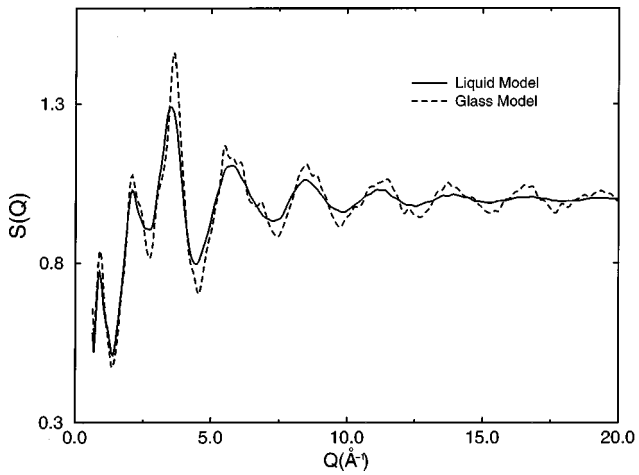

FIG. 1. The total static structure factors for liquid (solid line) and glass (dashed line) models.

Comparing the total and partial static structure factors of our liquid and glass models reveals a general trend of thermal broadening in all of the liquid peaks (Fig. 2). An approximate length scale of $2\pi/Q$ can be determined for the first three peaks at 0.93, 2.08, and 3.48 Å^{-1}, thus the peaks are associated with IRO ($\approx$6.0 Å), next-nearest-neighbor, and nearest-neighbor correlations, respectively. The first three peaks of the $S_{\alpha\beta}(Q)$'s decrease by about 10–15 % and the general trend of thermal broadening continues into the peaks at higher values of Q. The decrease in intensity is consistent with the neutron-scattering results of Ref. 3. The exception is the FSDP of $S_{\text{SeSe}}(Q)$ which remains unchanged. These results suggest that the covalent network is well formed in the liquid and that the IRO has almost completely emerged several hundred degrees above the glass transition temperature. The insensitivity of the $S_{\text{SeSe}}(Q)$ FSDP to temperature lends further support to this view. The $S_{\text{SeSe}}(Q)$ FDSP must depend on correlations between Se that are part of $\text{Ge}(\text{Se}_{1/2})_4$ tetrahedra within a well formed network of such tetrahedra.

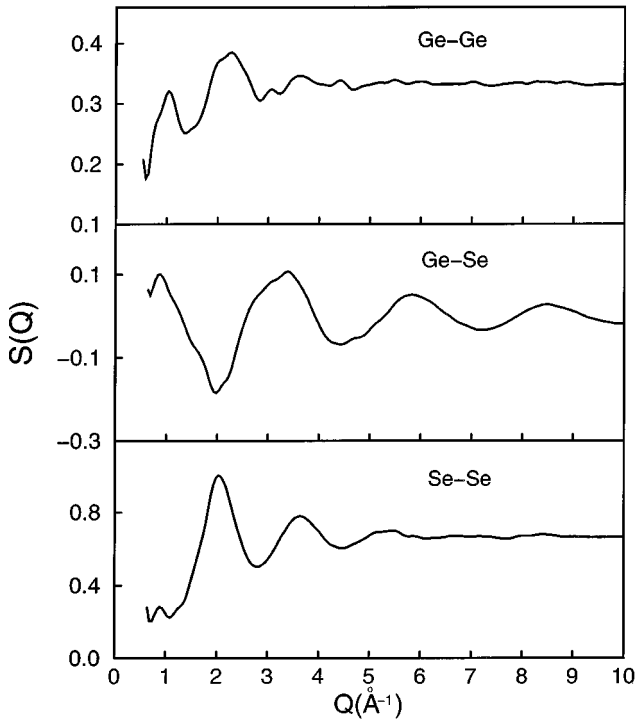

FIG. 2. The average partial static structure factors for liquid model.

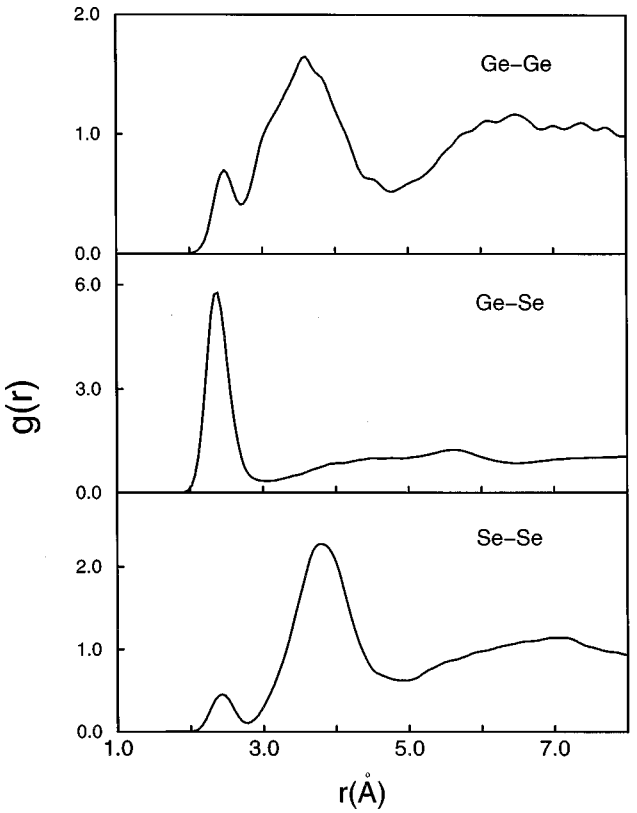

FIG. 3. The average partial pair-correlation functions for liquid model.

B. Pair-distribution functions, angle distribution functions, and ring statistics

Partial pair-distribution functions (PDF's), angle distributions, and ring statistics are used to determine the topology of our model. We find that our partial pair-distribution functions (Fig. 3) are in good agreement with those of Ref. 5 obtained from neutron-scattering data. In particular the fraction of homopolar (or ''wrong'') bonds is in very good agreement with the experimental $g_{\text{SeSe}}(r)$ and $g_{\text{GeGe}}(r)$ results, therefore it is possible to obtain a good estimate of the chemical disorder in l-GeSe_2. Mössbauer experiments, using Sn and Te as Ge and Se probes, respectively, have shown that Ge and Se wrong bonds exist in g-GeSe_2 (Refs. 17,18). The fraction of Ge atoms not tetrahedrally coordinated by Se atoms was determined to be about 16% in these experiments, but the fraction of Se wrong bonds has not yet been determined from Mössbauer measurements. The angle distributions (Fig. 4) and ring statistics (Table I) provide information about the $\text{Ge}(\text{Se}_{1/2})_4$ tetrahedra and the configurations they form. This kind of three-dimensional information can only be obtained from a microscopic model such as ours and is essential to understanding the network topology of the liquid and glass.

From the $g_{\text{SeSe}}(r)$ distribution we find that the average Se-Se bond length is about 2.43 Å and the average next-

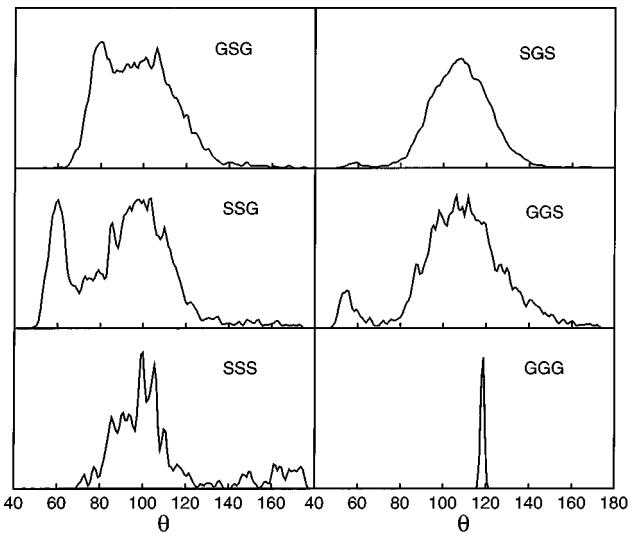

FIG. 4. The average angle distributions for liquid model.

nearest-neighbor distance is about 3.8 Å. The fraction of Se with wrong bonds is about 24%. About 18% of these are part of dimers and 6% are part of trimers. The fraction of onefold Se atoms is around 15% and the fraction of threefold Se atoms is around 23%. The next-nearest-neighbor peak can be associated with correlations between Se atoms which share a Ge atom and correlations between Se atoms on neighboring tetrahedra which do not share a Ge atom. We find that the average number of next-nearest Se neighbors is about 10.40 [with a cutoff near the appropriate minimum in $g_{\mathrm{SeSe}}(r)$ at 4.9 Å] which is very close to the value of 10.35 obtained in Ref. 5. The peak around 7.0 Å is an indication of the IRO in our model. It is apparent from Fig. 4 that the Se-Se-*B* (*B* being a Se or Ge atom) have their central peaks around 101° which is quite close to the Se-Se-Se angle of 103° in trigonal selenium (Ref. 19). The Ge-Se-Se peak around 60° is due to threefold rings. The number of Ge-Se-Se angles less then about 78° increased by about a factor of 3 in the liquid and the peak around 60° has increased by about 50% over its value in the glass.

The $g_{\mathrm{GeSe}}(r)$ distribution gives an average bond length of 2.37 Å which is close to the experimental result of 2.42 Å. The average number of Se neighbors is around 3.60 (for a cutoff of 2.86 Å). This coordination number is quite close to the experimental value of 3.63 obtained in Ref. 5. The fraction of undercoordinated Ge atoms is 16%, of overcoordinated Ge atoms is 8%, and of Ge in $\mathrm{Ge(Se_{1/2})_4}$ tetrahedra is about 58%. The peak around 5.6 Å is further evidence of IRO in our model. The Ge-Se-Ge angle distribution has two main peaks around 80° and 100° which correspond, respectively, to edge and corner sharing tetrahedral configurations. From the Se-Ge-Se angle distribution it is apparent that the average tetrahedral angle is about 109°, the ideal tetrahedral angle.

We find the average Ge-Ge bond length of our model to be about 2.48 Å. The fraction of Ge atoms with homopolar bonds is 26 with 24% of these in ethane dimers and the other 2% in trimers. The second peak at 3.6 Å is the result of edge and corner sharing tetrahedra; Ge atoms which share one Se atom are corner sharing and Ge atoms which share two Se atoms are edge sharing. The corner sharing tetrahedra are responsible for most of the second peak's intensity. We find that the edge sharing tetrahedra account for the shoulder around 3.08 Å. The ratio of edge to corner sharing tetrahedral configurations is around 50% which is consistent with the experimental results of Ref. 5. In addition the average number of next-nearest neighbors is 3.40 (for a cutoff of 4.4 Å) which is close to the value of 3.36 obtained in Ref. 5. The presence of IRO is seen again in the peak structure between 5.0 and 8.0 Å. The Ge-Ge-Se angle distribution has a peak around 109° and is quite similar to the Se-Ge-Se angle distribution. The Ge-Ge-Ge trimers form tetrahedronlike angles as well with a peak at 119°. It appears that the strong sp^3 bonding hybridization of the Ge atoms creates tetrahedronlike angle distributions.

The ring statistics in Table I show that fourfold and sixfold rings are about twice as numerous as other types of rings of order less then 10. Because short- and intermediate-range ordering effects dominate in l-$\mathrm{GeSe_2}$ the fourfold and sixfold rings appear to be the dominant ring structures of our model. The fourfold rings are all formed from edge sharing tetrahedra and about 86% of the sixfold rings contain three Se atoms which suggests that they are formed from corner sharing tetrahedra. Because of chemical disorder it is possible to form sixfold rings which have Se-Se and Ge-Ge bonds. The fivefold rings can only exist when there is chemical disorder. In our previous study of the glass (Ref. 2) we found all of the fourfold rings were formed from edge sharing tetrahedra and that 82% of the sixfold rings are formed from corner sharing tetrahedra. These results indicate that the majority of sixfold rings in the liquid are chemically ordered. The average number of fourfold and sixfold rings only differ from their values in the glass by about 20%. There are a number of highly strained threefold rings formed from corner sharing tetrahedra and Se-Ge-Se angles on individual tetrahedra. The very small angles in the Se-Ge-Se, Ge-Se-Ge, Se-Se-Ge, and Se-Ge-Ge angle distributions can be associated with these threefold rings.

C. The role of fourfold and sixfold rings in determining the intermediate range order

The IRO of the liquid and glass phases of $\mathrm{GeSe_2}$ can clearly be seen in the total static structure factor and the partial pair-distribution functions. In addition it has been observed in theoretical studies of the glass that there is a strong correlation between the fraction of edge sharing tetrahedra (fourfold rings) and the intensity of the FSDP (Refs. 2,20). As the fraction of edge sharing tetrahedra approaches a value of about 40% the FSDP reaches its maximum intensity (Ref.

TABLE I. Average ring statistics. Average number of n-order rings, $n=3$ through $n=12$.

Ring size	3	4	5	6	7	8	9	10	11	12
Number of rings	10	23	11	20	6	13	9	15	25	35

2). Unfortunately this information provides only a vague idea about how the IRO manifests itself within the network topology.

Ordering on a length scale of about 6.0 Å in a covalent network implies that there are structures or density fluctuations of a similar length scale. The high-temperature form of crystalline $GeSe_2$ provides a useful model for understanding IRO correlations which might exist in liquid and glassy $GeSe_2$. In the high-temperature crystal phase of $GeSe_2$ interlayer and intralayer atomic correlations involving fourfold and sixfold rings determine the IRO (Ref. 7). The work of Fischer-Colbrie and Fuoss[7] demonstrates that a spherically symmetric model based on the high-temperature form of c-$GeSe_2$ is able to reproduce the experimental $S(Q)$ of g-$GeSe_2$ to a great extent. This strongly suggests that the crystal and the glass have very similar short-range and intermediate-range order at least in a spherically symmetric sense. The structural properties of our model indicate that a high degree of short- and intermediate-range order exists in the liquid near the melting point of the crystal. This suggests as well that the IRO which exists in the liquid and the glass is similar to that of the crystal. Therefore we would like to determine if the fourfold and sixfold rings (taken as point objects) in the liquid and glass are ordered on a length scale of about 6 Å. The simplest way to do this is to determine the partial $S(Q)$'s for fourfold (4-4), sixfold (6-6), and fourfold and sixfold (4-6) ring correlations within our liquid and glass models.

In order to determine the 4-4, 6-6, and 4-6 ring correlations, the center of mass of each fourfold and sixfold fold ring in our model was determined. We then calculated partial ring $S(Q)$'s, treating the CM's as a set of point particles. The $S_{44}(Q)$, $S_{66}(Q)$, and $S_{46}(Q)$ for our liquid and glass models are shown in Fig. 5. The main peak in all of these structure factors is around 1.0 $Å^{-1}$ which indicates that the fourfold and sixfold rings display very strong IRO correlations of about 6.0 Å. This is direct evidence of IRO in the correlations of fourfold and sixfold ring structures in liquid and glassy $GeSe_2$.

The peak around 1.0 Å in our ring $S(Q)$'s implies that atoms which are part of these rings should contribute significantly to the FSDP of the liquid and glass $S(Q)$. In order to demonstrate this we have eliminated correlations between atoms in fourfold rings [Fig. 6(a)], sixfold rings [Fig. 6(b)], and all of the correlations between 4-4, 6-6, and 4-6 ring atoms [Fig. 6(c)] within a range of 4.6 to 9 Å in the total $S(Q)$ of our glass model (Fig. 1). The range over which correlations were eliminated was determined from the Q values at which the FSDP begins and ends. The resulting total $S(Q)$'s no longer have an FSDP, although the when the fourfold ring correlations are eliminated a slight shoulder persists. This is consistent with our ring correlation functions which indicate that 4-6 and 6-6 ring correlations should be more intense then the 4-4 ring correlations. When all the correlations are eliminated the effect is more intense then the elimination of just the 4-4 and 6-6 ring correlations together indicating that the 4-6 correlations are an important part of the FSDP as well. As an additional test of this approach we eliminated the correlations of the fivefold ring atoms with themselves (Fig. 7) and found that the FSDP was stillpresent. One might expect this since fivefold rings would not exist in

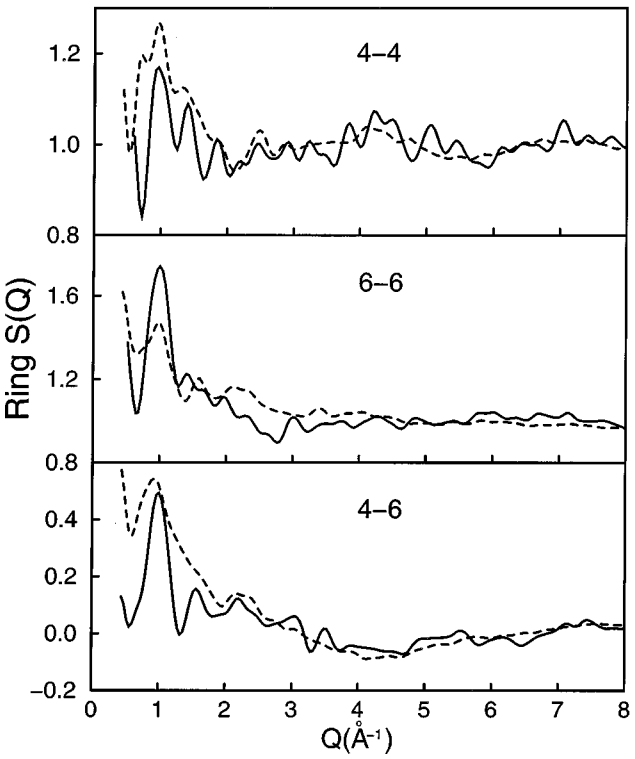

FIG. 5. Ring static structure factors for 216 atom liquid (dashed line) and glass (solid line) models.

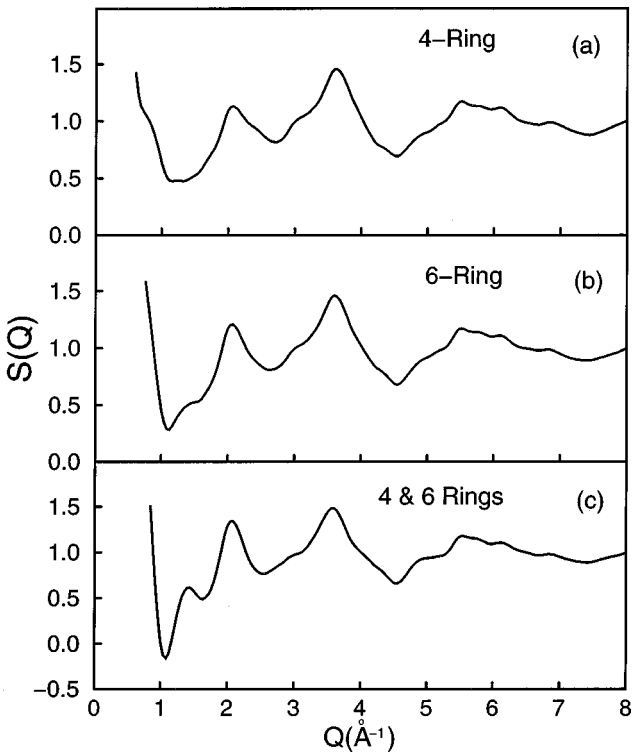

FIG. 6. The total static structure factor for 216 atom glass model with all the 4.6–9.0 Å (a) correlations between atoms in fourfold rings eliminated, (b) correlations between atoms in sixfold rings eliminated, and (c) correlations between fourfold, sixfold, and fourfold and sixfold rings eliminated.

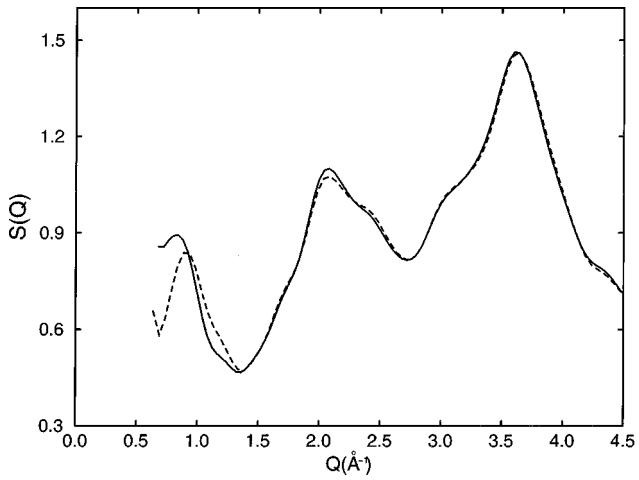

FIG. 7. The total static structure factor for 216 atom glass model with all the 4.6–9.0 Å correlations between atoms in fivefold rings eliminated (solid line) and the total static structure factor of the 216 atom glass model (dashed line).

a chemically ordered sample of g-$GeSe_2$ and thus cannot possibly be the structural origin of the FSDP. This is further evidence that the fourfold and sixfold rings are a crucial part of the IRO. It should be pointed out that we do not examine the elimination of correlations between chemical species since the FSDP is present in Se-Se, Ge-Se, and Ge-Ge correlations (Fig. 2).

All of these results taken together suggest that fourfold and sixfold rings play an important role in the IRO of the liquid and the glass and that the IRO is similar to that of crystalline $GeSe_2$. There could be other IRO correlations but because the fourfold and sixfold ring atoms account for 68% of all the atoms in the glass model they are probably the dominant form of IRO. Because of chemical disorder and coordination defects about 25% of the atoms in the glass model do not take part in fourfold, fivefold, or sixfold rings but it is unlikely that correlations between these atoms would play a significant role in the IRO. In a well annealed sample of g-$GeSe_2$ such defects would not exist to any great extent and the dominant tetrahedral configurations would be fourfold and sixfold rings. The IRO of liquid and glass $GeSe_2$ has been characterized through fourfold and sixfold ring correlations.

The IRO of the ring correlations also suggests an explanation for the glass-forming ability of $GeSe_2$. Structural similarities in the short- and intermediate-range order of the crystal, liquid, and glass could explain why $GeSe_2$ is such a good glass-forming material (Ref. 21). A good glass-forming material can be bulk quenched as opposed to evaporation deposited to form a disordered network. These two methods of forming glasses have very different time scales and therefore allow different amounts of structural disorder as the glass forms. The good glass-forming ability of $GeSe_2$ indicates that the glass shares some topological similarities with the crystal which allow both the glass and the crystal to emerge from the liquid state. These topological similarities would have to be rather general since the glass does not have the two-dimensional layer structure of the crystal and yet still constrains the short and IRO of the glass to be like that of the crystal in three dimensions. The short-range order is almost identical in the crystal and the glass and because of the fourfold and sixfold ring correlations the crystal and the glass would have very similar IRO topological constraints. These similarities could make it easier to form the glass from the liquid because less structural *disorder* would have to be preserved (or created) when the liquid is quenched to the glass state.

Evidence that short- and intermediate-range order similarities between the crystal, liquid, and glass affect the glass-forming ability of Ge-Se alloys can be found in comparisons between $GeSe_2$ and GeSe. Germanium selenide is the only other Ge-Se alloy which forms a crystal but it is a very poor glass former. The structural properties of GeSe are quite different from $GeSe_2$ in that the liquid and glass states have very weak FSDP's (and thus much less IRO) and the crystal and glass states are structurally quite different even in their short-range order. The short-range order of the low-temperature crystal phase of GeSe is closer to that of l-GeSe than that of g-GeSe (Refs. 22,23). All of these facts suggest that the glass-forming ability of GeSe and $GeSe_2$ is determined by the similarity of the short- and intermediate-range order of their liquid, glass, and crystal phases. Experimental work by Salmon and Liu (Ref. 22) shows quite clearly that the IRO of Ge_ySe_{1-y} liquid alloys decrease as y increases from 0.33 to 1. They find that the FSDP of l-GeSe is almost gone and in order to create glassy GeSe very fast methods such as sputtering or evaporation deposition must be used. This data shows a strong connection between the short- and intermediate-range order of the crystal, liquid, and glass phases of GeSe and $GeSe_2$ and their glass-forming ability. It also supports our view that the crystal, liquid, and glass phases of $GeSe_2$ have very similar intermediate-range order determined to a great extent by fourfold and sixfold rings.

IV. VIBRATIONAL PROPERTIES

The vibrational density of states (VDOS) $g(\omega)$ of a liquid can be obtained from the Fourier transform of the velocity autocorrelation function

$$C(t)=\frac{\langle \mathbf{V}(0)\cdot\mathbf{V}(t)\rangle}{\langle \mathbf{V}(0)\cdot\mathbf{V}(0)\rangle}, \tag{1}$$

$$\langle \mathbf{V}(0)\cdot\mathbf{V}(t)\rangle=\frac{1}{3N}\sum_{i}^{N}\sum_{j}^{3} V_{ij}(0)V_{ij}(t), \tag{2}$$

$$g(\omega)=\frac{2}{\pi}\int_0^T C(t)\cos(\omega t)W(t)dt. \tag{3}$$

The values of N and T are the number of atoms and the total simulation time, respectively. The summations in Eq. (2) are over the total number of atoms and the three components of each atom's velocity. We use a standard Blackman window

$$W(t)=0.42+0.5\cos\left(\frac{\pi t}{T}\right)+0.08\cos\left(\frac{2\pi t}{T}\right) \tag{4}$$

for $W(t)$ (Ref. 24). The spectral resolution of the Fourier transform depends on how much time series data can be generated. We were able to generate continuous 3.5 ps long

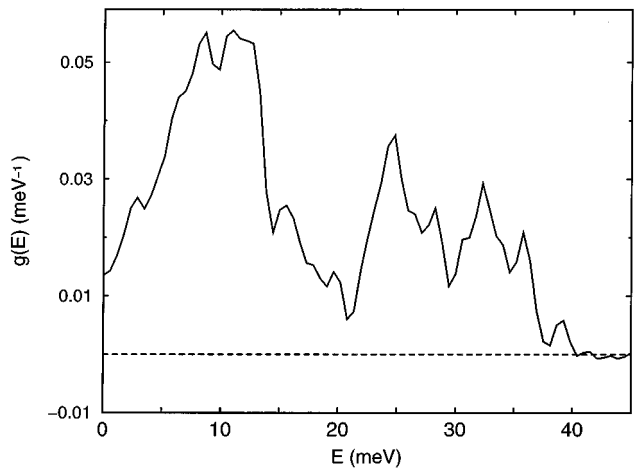

FIG. 8. The vibrational density of states for liquid model.

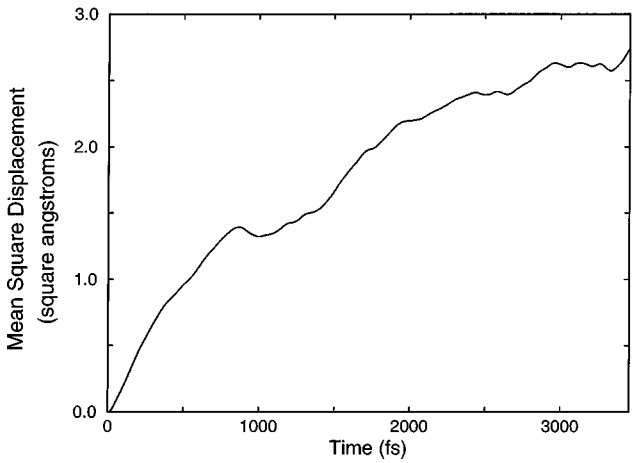

FIG. 9. The mean-square displacement of atoms in liquid model.

trajectories with a time step of 3.5 fs. This simulation provided us with a VDOS that has a spectral resolution of 0.58 meV. The fine structure of the Fourier transform also depends on the window function used. We found that the Blackman window gave the best results over the entire spectral range of our VDOS.

It is apparent from the experimental Raman-scattering results of Magna and Lannin (Ref. 8) that the liquid VDOS is similar to that of the glass. The Raman results indicate that the liquid and glass are quite similar below 19 meV, that there is a weakening of the A_{1c} (26.5 meV) peak, and that there is a significant reduction in the intensity of the high-frequency band. Our VDOS (Fig. 8) has the same qualitative features as the experimental results, particularly the weakening of the A_{1c} peak relative to the A_1 (24.8 meV). Our VDOS has more structure then the experimental data in the vicinity of the A_{1c} and perhaps the shoulder peak at 26.5 meV and the peak at 28.3 meV should be interpreted as the total A_{1c} band. The high-frequency band has two main peaks at 32.3 and 35.7 meV and there is a significant decrease in liquid VDOS intensity relative to the glass VDOS beginning around 32 meV in agreement with experiment.

Although it is impossible to determine harmonic modes of the liquid VDOS it is possible to make inferences based on the normal modes of the glass VDOS. In our previous paper (Ref. 2) we found that the low-frequency modes were very extended modes which involved the motion of tetrahedral units. We were able to determine that the A_1 and A_{1c} bands of the glass involved tetrahedral breathing and the motion of Se atoms joining edge sharing tetrahedra, respectively (Ref. 25). The third main peak of the glass VDOS contained many modes which involved F_2-type motion of tetrahedra (Ref. 26). The similarities in the structure of the liquid and the glass suggests that the underlying dynamics of the three main liquid VDOS bands are essentially the same as those in the glass. The decrease in the spectral intensity of the higher frequency band could be attributed to a loss of network rigidity required for such complex intratetrahedral motion. The same argument could be made too for the weakening of the A_{1c} peak. These types of coherent motion require a reasonably rigid network. This would also explain why the intensities of the low-frequency band and the A_1 peak do not decrease in the liquid. These types of dynamics require only individual tetrahedral units, but do not require a high degree of network rigidity. In particular the A_1 breathing modes have a high degree of spherical symmetry which make them very insensitive to thermal effects, while the A_{1c} and F_2 modes are highly planar in there motions which must surely make them more sensitive to network distortions.

The self-diffusion constant of l-$GeSe_2$ can be determined from the zero-frequency value of $g(\omega)$ using the standard expression (Ref. 27)

$$D=(1/3)\int_0^\infty \langle \mathbf{V}(0)\cdot\mathbf{V}(t)\rangle W(t)dt. \tag{5}$$

The diffusion constant obtained from $g(0)$ has a value of 1.6×10^{-5} cm^2/s. The low value of D indicates that the system is near the melting temperature of the crystal. We also found that $g(0)$ was quite insensitive to the type of window function used. The mean-squared atomic displacement (Fig. 9) provides an alternate approach for obtaining the value of D. It can be seen from Fig. 9 that the system is in a diffusive state beyond $t=1000$ fs. Assuming the Einstein relation for self-diffusion holds beyond $t=1000$ fs (Ref. 27)

$$\langle (r(t)-r(0))^2\rangle = 6Dt. \tag{6}$$

Fitting the diffusive part of Fig. 9 with a straight line we obtain a value of 1.0×10^{-5} cm^2/s for D. Both of these approaches for obtaining D suffer from the short time scales of our model and perhaps give an upper and lower bound on the actual value of D. Although our total simulation time is relatively short (3.5 ps) the VDOS appears to be in reasonable agreement with the experimental data and the mean-squared atomic displacement curve is essentially linear for the latter two thirds of the simulation. Both of these results indicate that our liquid model reached a state of equilibrium early in the simulation and that the simulation time was sufficiently long enough to properly model the dynamics of l-$GeSe_2$.

V. ELECTRONIC PROPERTIES

In this last section we examine the electronic properties of liquid $GeSe_2$. The electronic and optical properties of g-$GeSe_2$ (photoluminescence, light-induced electron-spin

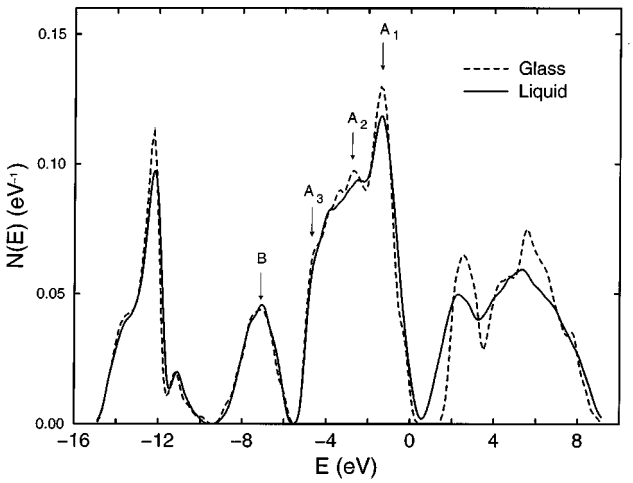

FIG. 10. The electronic density of states for liquid (solid line) and glass (dashed line) models.

resonance, photoinduced structural changes) have been studied quite extensively through experiments, but little progress has been made on theoretical interpretations of these results since the works of Kastner, Street, and Mott in the 1970's (Refs. 28–30). Two of the most important unresolved questions are the origin of the light-induced ESR (LESR) signal and the electronic states responsible for photoluminescence in g-$GeSe_2$. Photoluminescence and optical absorption experiments indicate that there are a significant number of states near the middle of g-$GeSe_2$'s optical gap (Refs. 11,31). It is believed that defect states, created as a result of optical excitations, produce the ESR signal but the details of these defects are still not well understood. In addition two distinct LESR signals have been identified and it is believed that they are the result of Ge and Se coordination defects, respectively. This is in contradiction with our earlier studies of g-$GeSe_2$ (Refs. 1,2) in which we found that there were no states in the optical gap despite the large number of topological defects in our models. It should be noted that the observed LESR spin density ($\approx 10^{15}$–10^{17} cm^{-3}) implies that we would need a glass model with about 10^6 atoms to see even one such defect (Refs. 10,11). A key finding of this work is that transient defect states pass through the liquid optical gap, similar phenomena may well occur (rarely) in the glass. Another important observation involving the asymmetric broadening of the valence- and conduction-band edges sheds new light on the issue of midgap states as well. The midgap states of our liquid model give us an opportunity to understand in a more fundamental way than previously possible the photoluminescence and the LESR observed in g-$GeSe_2$.

Microcanonical molecular dynamics were performed on our model to obtain average values of various physical quantities. The electronic density of states (EDOS) in Fig. 10 was obtained from such an average. The positions of the first four peaks below the Fermi level are listed in Table II. We find that there is little change in the positions of these four peaks relative to our results for the glass. The intensities of the first three peaks have decreased (relative to the glass) and the B peak intensity is unchanged. Because the B peak is associated with Ge s states one would expect it to be less sensitive to thermal effects. The Ge s states are less sensitive to bond angle distortions because of their spherical symmetry. The average total electronic localization and the average Ge and Se electronic localization are plotted in Fig. 11 (for more details on the electronic localization see Ref. 2). We find that the lowest two peaks of the EDOS, which are associated with Se and Ge s states, are localized on Se and Ge atoms, respectively. The localization of the valence-band peak is quite low but it increases near the optical gap. This is to be expected since the valence band is primarily associated with Ge sp^3 and Se p bonding states. The valence-band edge is associated with Se lone pair states and as see from Fig. 11 the localization is essentially on Se atoms. There is a small amount of localization on undercoordinated Ge atoms at the valence-band edge as well. The two main peaks of the conduction band appear to be associated with Se and Ge antibonding states, respectively.

TABLE II. The positions of the A_1, A_2, A_3, and B peaks of the electronic density of states for our liquid model.

(eV)	A_1	A_2	A_3	B
Theory	−1.4	−2.5	−4.5	−7.0

In Fig. 12 the time evolution of the local-density-approximation (LDA) electronic eigenvalues is plotted near the optical gap. Plotting the rms of the thermal fluctuation of each eigenvalue with the average localization of each eigenvalue (Fig. 13) reveals that there is essentially a linear relationship between the thermal fluctuations of an eigenvalue and its localization. This means that an essentially static property (the localization of the LDA electronic eigenvalues) of the liquid is linearly proportional to a dynamical property (the rms time fluctuation of the LDA eigenvalues) of the liquid. The only part of the EDOS which does not follow this trend is the peak around −11 eV. In our glass model these states were associated with Se atoms which were overcoordinated and/or had homopolar bonds. These bonding configurations, as we will discuss further, appear to have been affected significantly by thermal distortions. This could account for the discrepancy in the RMS of these eigenvalues. In general though the degree of localization determines the sensitivity of an eigenvalue to thermal rearrangements of the

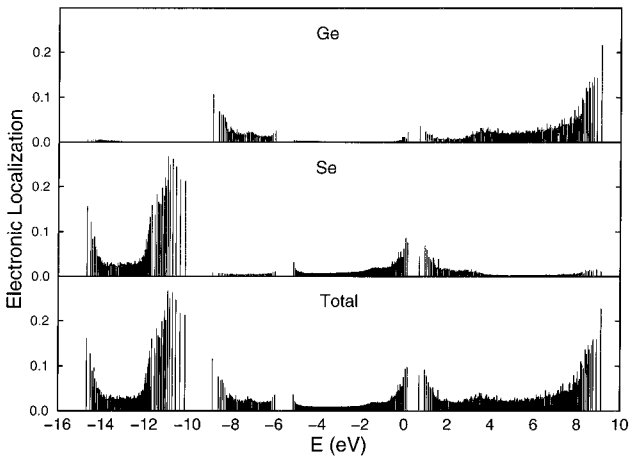

FIG. 11. The total average localization of the electronic eigenvalues and the average localization of the electronic eigenvalues on Ge and Se atoms.

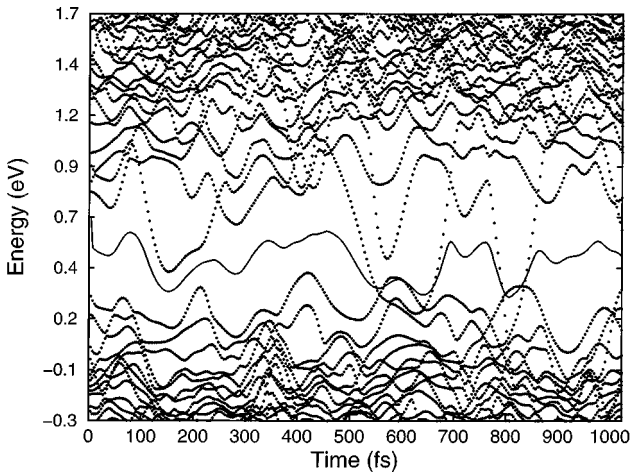

FIG. 12. The time evolution of the electronic eigenvalues (dotted lines). The Fermi level (solid line) is also plotted.

network topology. As the localization of an eigenvalue increases changes in the local network topology affect it to a much greater extent, and as the eigenvalue becomes more delocalized thermal affects are averaged out and the fluctuations of the eigenvalue decrease. This is clearly an example of the interaction between the electronic and ionic dynamics or in other words an electron-phonon interaction. Similar behavior has been observed by Drabold *et al.* in an *ab initio* study of *a*-Si (Ref. 9).

It is apparent from Fig. 10 that the liquid's optical gap is much smaller (0.45 eV) then the optical gap of the glass (1.72 eV) because the conduction band is broadened significantly and it is also apparent that the broadening of the valence and conduction bands is quite different. Comparing the broadening of the valence-band edge with the rms of its electronic eigenvalues [Fig. 13(b)] we find that thermal fluctuations are responsible for only about half of the total broadening of the valence band. The thermal fluctuations of the conduction-band-edge eigenvalues only account for approximately 1/3 of the total broadening of the conduction band. These results suggest that the total broadening of the valence

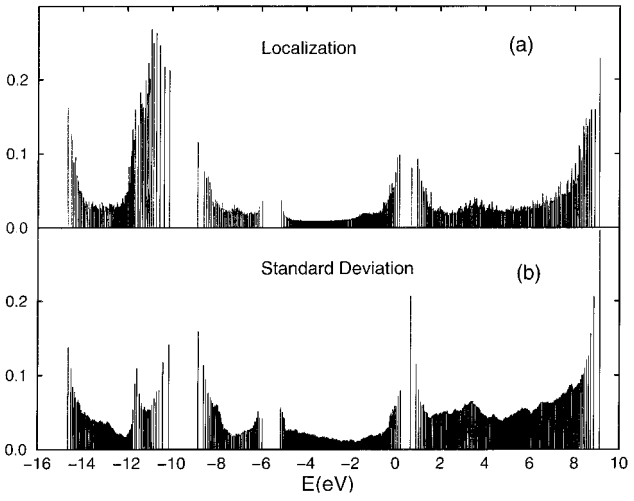

FIG. 13. (a) The average localization of the liquid's electronic eigenvalues and (b) the root mean square of the thermal fluctuations of the electronic eigenvalues in time.

and conduction bands is due not only to thermal fluctuations but intrinsic topological disorder as well. Electrical conductivity measurements (Ref. 32) reveal that the conductivity of Ge-Se melts is much lower at compositions which easily form glasses (such as $GeSe_2$) suggesting that a covalent network exists in these melts and that these compositions have optical gaps of 1–2 eV at temperatures several hundred degrees above the glass transition temperature. This study also finds that the conductivity of good glass-forming Ge-Se alloys increases quite rapidly (by several orders of magnitude) above 923 K indicating that the covalent network is broken down to a much greater extent above this temperature.

The difference in the broadening of the valence and conduction bands can be explained in part through the different chemistry associated with each band edge. In our earlier study (Ref. 2) we determined that the top of the valence band was associated with threefold Ge atoms, twofold Se atoms forming Se dimers, and onefold Se atoms. We also determined that the conduction-band edge was associated with threefold Se atoms to a large extent. The liquid's valence and conduction bands are associated with the same kind of bonding configurations. In particular we find that the liquid's conduction-band edge is associated with threefold Se atoms that have distorted *A*-Se-*B* angles (Se-Se-Ge angles $<78°$ and Ge-Se-Ge angles $>140°$) and/or stretched Se-Se and Ge-Se bonds (>2.6 Å). Overall there are not tremendous differences between the angle distributions of the liquid and the glass except for the number of distorted Se-Se-Ge angles $<78°$ which increased by about a factor of 3 in the liquid. Another important difference between the liquid and the glass is that stretched Se-Se bonds did not exist in our glass model. These facts suggest that threefold Se atoms in highly stressed configurations are responsible for the broadening of the conduction band.

It is of particular interest that the liquid has transient electronic states in the middle of its optical gap. It is likely that the midgap states in our liquid model and those observed experimentally in the glass are a result of similar structural configurations. It appears that in our liquid model the splitting between the nonbonding and antibonding Se states has been weakened in these topologically distorted threefold Se configurations. In order to test this hypothesis we created artificially stretched threefold Se bonds in our glass model. Using a conduction band state that was localized on a *threefold* Se atom we stretched a bond of this Se atom. As the stretching increased the conduction band state moved across the optical gap until it was just above the valence-band edge. The Fermi level in our glass model is located just above the valence-band edge. Stretching the bond (bond length 2.41 Å) 0.55 Å shifted the energy of the conduction-band state -1.4 eV (or about 0.4 eV/Å). Because g-$GeSe_2$ has a relatively low density it was possible to stretch bonds without forcing atoms to become unphysically close. The behavior of these artificial defect states is consistent with what we observe in the liquid. The conduction-band states are much more sensitive then the valence-band states to topological distortions because the formation of a threefold Se atom involves the destruction of a lone pair p state in order to create an additional bonding state. Thus one would expect these threefold Se states to be more sensitive to topological distortions since the Se atom would prefer to be twofold coordi-

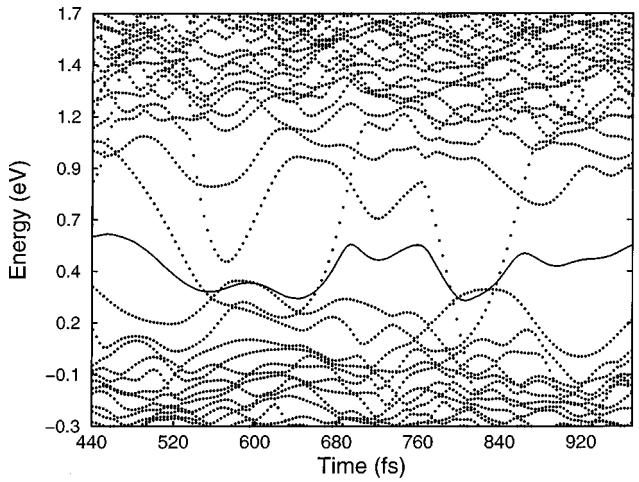

FIG. 14. Energy level crossing events (dotted lines) and the Fermi level (solid line).

nated with a lone pair state. The bonding configurations associated with the valence band are much less sensitive to topological disorder since they do not involve the creation or destruction of lone pair states. In addition the conduction-band state moves towards the valence band because it is becoming more like a lone pair state. The top of the valence-band edge is, as mentioned previously, associated with Se lone pair states.

We observed four gap crossing events in our thermal simulation, for which the valence- or conduction-band energy levels crossed the 0.45 eV optical gap. In each event either the valence band ascended into the optical gap or the conduction band descended into the optical gap as seen from Fig. 14 creating a transient midgap state. The energy level then proceeded to cross the nearest level and sometimes continued to ascend or descend. The duration of each of these four events was (in order of appearance in Fig. 14) 94.5, 49, 35, and 24.5 fs. It should be noted that a valence-band state cannot cross the gap (and the Fermi level) unless a conduction-band state has already come down so that the number of electrons is conserved. The Fermi distribution function is smeared out near the Fermi level at finite temperatures so that the valence and conduction bands can both be partially occupied in these level crossing events. The smearing of the Fermi function allows the conduction band to descend while conserving the number of electrons. It is rather difficult to discern all these details from Fig. 14 but as we will discuss it is possible to track the energy eigenstates through the atoms which they localize on. The manner in which these midgap states are created is different from experimental techniques of optically annealing g-$GeSe_2$ but the structural information they provide about the midgap states is still relevant.

The structural origin of these band crossings was determined from the localization of the electronic eigenvalues as they passed through the optical gap. In each event between two and five atoms had significant localization and all of these atoms were nearest or next-nearest neighbors. We were able to isolate the common traits of these events through visualization and detailed analysis of how each atom's bonding environment changed during the gap crossing. As the eigenvalues pass through the gap the bonding of the atoms associated with each eigenvalue change from valence- to conduction-band states or vice versa depending on which way the eigenvalue is moving. The bonding configurations of the atoms involved transform from valence- (conduction) to conduction- (valence) band states, two examples of this being a onefold Se becoming a twofold Se and a twofold Se becoming a threefold Se (see Table III). Some of the atoms involved do not undergo a change in their bonding but are merely the nearest neighbors of atoms which are changing their bonding configurations. In addition to the Se atoms, the electronic states localize on Ge atoms making or breaking bonds with the Se atoms involved. These events are the dynamic version of what we observed in the broadening of the conduction band and from them it can be concluded that midgap states are generated by Se atoms which form weak bonds with their Se and Ge neighbors. They are not really valence- or conduction-band states, but rather an intermediate state between the two. A simple interpretation of these events is that the lone pair states of the Se atoms are being unoccupied (occupied) as the energy levels cross from the valence (conduction) band to the conduction (valence) band. When the lone pair states become unoccupied (occupied) an antibonding state is created (destroyed) and a bonding state is created (destroyed) as well. This interpretation is consistent with our explanation for the broadening of the conduction-band edge and with the high percentage (78%) of transient gap states which involve threefold Se.

Previous experimental work on glassy $GeSe_2$'s electronic and optical properties have focused on photoluminescence, optical absorption, LESR signals, dc conductivity, and photoconductivity. Optical excitations should induce the creation of defect states in the valence and conduction bands as structural relaxations occur due to the displacement of charge. It

TABLE III. When an electronic state crosses the optical gap we find that it is localized on a small number of neighboring atoms. Listed below are the localized structural changes we observe as electronic states cross from the valence (conduction) band to the conduction (valence) band. The neighbors of an atom are in parentheses. 3Se indicates that a Se neighbor is threefold coordinated.

Valence band → Conduction band	Conduction band → Valence band
Se(Ge) → Se(Ge,Ge)	Se(Ge,Ge) → Se(Ge)
Se(Ge,Ge) → Se(Ge,Ge,Ge)	Se(Ge,Ge,Ge) → Se(Ge,Ge)
Se(Ge,Se) → Se(3Se,Se,Ge)	Se(Se,Ge,Ge) → Se(Ge,Ge)
	Se(3Se,Ge) → Se(Ge)
Ge(3Se,Se) → Ge(3Se,3Se,Se,Se)	Ge(3Se,3Se,3Se,Se,Se) → Ge(3Se,3Se)

is impossible for us to make direct comparisons with experiment since we are not simulating dynamic optical interactions, although much can be inferred about the structural details of such defects from our liquid results. Based on experimental results it has been speculated that photoluminescence and LESR in g-$GeSe_2$ are the result of Se and Ge dangling bonds (Refs. 10,11,30). Our results strongly support this view and give a much clearer picture of the exact structural nature of these dangling or stretched bond states. In particular we can explain the prescence of Se and Ge LESR signals in terms of the states we observe moving through the optical gap. When g-$GeSe_2$ is exposed to band-gap wavelength light Se and Ge ESR signals are produced. Both LESR signals are holelike which indicates that they are being produced by neutral dangling bond states. Neither LESR signal saturates but rather each reaches an equilibrium value determined by the wavelength and intensity of the incident light. When the light is turned off the system freezes into its equilibrium ESR value (Ref. 11). The equilibration of the ESR signal indicates that a dynamic process is creating and destroying these dangling bond states.

The different types of dangling bond configurations we observe moving through the optical gap represent some of the different ESR neutral defects that could be created from optical excitations. The stretched bond configurations detailed in Table III indicate the different types of neutral defects that occur in our liquid model. Experimentally it is known that *light-induced* ESR does not occur in amorphous Ge and Si suggesting that lone pair electrons are the mechanism through which optically induced defects occur in chalcogenides. The lone pair electrons would be optically excited into the conduction band resulting in the creation of defect states. These experimental results support our interpretation of the midgap states observed in the liquid model.

It is well known that the LESR signal in g-$GeSe_2$ can be completely erased by annealing a sample around 400 K (Ref. 11). Experiments also reveal that annealing a g-$GeSe_2$ sample around 100 K will erase a light-induced Se ESR signal but that a temperature of about 300 K is required to erase a light-induced Ge ESR signal. Based on our study of g-$GeSe_2$ this effect would be consistent with a decrease in structural and chemical disorder. We observed significant localization on Se dimers at the edge of the valence and conduction bands in g-$GeSe_2$. In addition we also found localization on onefold Se and threefold Ge near edge of the valence band. Experimental results on g-$GeSe_2$ evaporation deposited thin films indicate that the optical gap increased as a result of annealing and that the chemical disorder of the thin films decreased after being annealed (Refs. 31,33,34). This suggests that the chemically ordered Ge-Se stretched bonds anneal at higher temperatures. We also observe Se-Se stretched bond states moving across the optical gap of the liquid indicating that such states could contribute to the Se LESR signal.

Experimental photoluminescence data for g-$GeSe_2$ suggests that there is more than one type of optical transition occurring. The photoluminescence peak has a full width at half maximum of about 0.3 eV and its position depends on the excitation energy (Ref. 11). This is consistent with the variety of energies at which we observe gap states in the optical gap of the liquid. Our results also suggest that the observed pinning of the Fermi level (Ref. 31) is a result of occupied (onefold and twofold Se) and unoccupied (threefold Se) dangling bond states near the middle of the optical gap. In the actual glass these would presumably be intrinsic defects formed during the glass transition.

VI. CONCLUSION

The structural, vibrational, and electronic properties of l-$GeSe_2$ have been analyzed using *ab initio* molecular dynamics. We find that the average topology of our liquid model is in excellent agreement with experimental results as evidenced by the total and partial static structure factors as well as the partial pair-distribution functions. In particular the FSDP of the total static structure is in excellent agreement with experiment indicating that the IRO is well described by our model. The average bond lengths, number of nearest and next-nearest neighbors, percentage of wrong bonds, and the ratio of edge to corner sharing tetrahedra are all in very good agreement with experiment as well.

We have introduced a method of characterizing the IRO of liquid and glassy $GeSe_2$ using the fourfold and sixfold ring structures which exist in liquid, glassy, and crystalline $GeSe_2$. Treating the fourfold and sixfold rings as point objects we have shown that they exhibit IRO correlations similar to ring correlations which exist in the high-temperature crystalline form of $GeSe_2$. In addition we have shown that the atomistic correlations associated with these ring structures are an essential part of the static structure factor's FSDP. This data strongly suggests that the FSDP's of liquid and glassy $GeSe_2$ are a result of the IRO imposed by fourfold and sixfold ring correlations.

The vibrational density of states of our liquid model is in very good qualitative agreement with Raman experiments. We find that the intensity of the low-frequency peak is quite similar to that of the glass and that the intensity of the high-frequency peak is significantly reduced relative to its intensity in the glass. In addition the splitting of the A_1 and A_{1c} peaks and the reduced intensity of the A_{1c} peak in the middle band are reproduced in agreement with experiment. We hope this calculation inspires someone to attempt neutron-scattering measurements of liquid $GeSe_2$ which we could then make direct comparisons with.

We find that the average EDOS of the liquid is quite similar to the EDOS of the glass below the Fermi level. Above the Fermi level we find that localized topological distortions result in a very significant broadening of the conduction band. Examining the time-dependent behavior of the electronic eigenvalues we find that the rms of their thermal fluctuations is linearly proportional to their average localization. This suggests to us that the more localized an eigenvalue is, the greater its sensitivity to thermal distortions in the local network topology.

From our observations of electronic eigenvalues crossing the optical gap of the liquid we find that a variety of bonding configurations can produce these midgap states. This is an observation of these femtosecond gap crossing events in l-$GeSe_2$. Recent advancements in femtosecond x-ray techniques open up the possibility of studying structural changes

occurring on the femtosecond time scale (Refs. 35,36). Therefore it may be possible in the near future to actually observe the structural transformations responsible for these gap states as well as measure changes in the electronic structure on the femtosecond scale. In addition these liquid gap states have structural properties similar to gap states in the glass observed through LESR and photoluminescence measurements. Our results suggest in agreement with experiment that Se lone pair states are the mechanism through which states in the optical gap are created. The creation and destruction of lone pair states appears to correspond with the movement of eigenvalues across the optical gap which suggests that a Se antibonding state is either being created or destroyed.

Overall we find that our liquid model is in very good agreement with experiment. It may in fact be in better agreement with experiment then our glass model. We believe this occurs because it is unnecessary to quench the liquid. Simulating the quenching process with femtosecond scales makes the resulting glass model more disordered then the real glass (Ref. 2). Nevertheless both models give very good descriptions of the two disordered phases of $GeSe_2$ and when used together provide new and unexpected results.

ACKNOWLEDGMENTS

The authors would like to thank Professor R. L. Cappelletti for many insightful discussions on liquid and glassy $GeSe_2$. This work was partially supported by NSF Grant No. DMR 96-18789.

[1] R. L. Cappelletti, Mark Cobb, D. A. Drabold, and W. A. Kamitakahara, Phys. Rev. B **52**, 9133 (1995).
[2] Mark Cobb, D. A. Drabold, and R. L. Cappelletti, Phys. Rev. B **54**, 12 162 (1996).
[3] S. Susman *et al.*, J. Non-Cryst. Solids **125**, 168 (1990).
[4] Osamu Uemura *et al.*, J. Non-Cryst. Solids **30**, 155 (1978).
[5] Ian T. Penfold and Phillip S. Salmon, Phys. Rev. Lett. **67**, 97 (1991).
[6] J. C. Phillips, J. Non-Cryst. Solids **43**, 37 (1981), and references therein.
[7] A. Fischer-Colbrie and P. H. Fuoss, J. Non-Cryst. Solids **126**, 1 (1990).
[8] J. R. Magna and J. S. Lannin, J. Non-Cryst. Solids **59&60**, 1055 (1983).
[9] David A. Drabold, P. A. Fedders, Stefan Klemm, and Otto F. Sankey, Phys. Rev. Lett. **67**, 2179 (1991).
[10] S. G. Bishop, U. Strom, and P. C. Taylor, Phys. Rev. B **15**, 2278 (1977).
[11] R. A. Street and D. K. Biegelsen, J. Non-Cryst. Solids **32**, 339 (1979).
[12] Otto F. Sankey and D. J. Niklewski, Phys. Rev. B **40**, 3979 (1989); Otto F. Sankey, D. A. Drabold, and G. B. Adams, Bull. Am. Phys. Soc. **36**, 924 (1991).
[13] G. B. Bachelet, D. R. Hamann, and M. Schlüter, Phys. Rev. B **26**, 4199 (1982).
[14] J. Harris, Phys. Rev. B **31**, 1770 (1985).
[15] Peter Fulde, *Electron Correlations in Molecules and Solids*, 2nd ed. (Springer-Verlag, New York, 1993), p. 44.
[16] Alexander A. Demkov *et al.*, Phys. Rev. B **52**, 1618 (1995).
[17] M. Stevens, P. Boolchand, and J. G. Hernandez, Phys. Rev. B **31**, 981 (1985).
[18] W. J. Bresser, P. Boolchand, P. Suranyi, and J. P. de Neufville, Phys. Rev. Lett. **46**, 1689 (1981).
[19] R. Martin, G. Lucovsky, and K. Helliwell, Phys. Rev. B **13**, 1383 (1976).
[20] P. Vashishta *et al.*, Phys. Rev. Lett. **62**, 1651 (1989).
[21] J. C. Phillips, J. Non-Cryst. Solids **34**, 153 (1979), and references therein.
[22] Philip S. Salmon and Jian Liu, J. Phys. Condens. Matter **6**, 1449 (1994).
[23] Dale E. Sayers, Farrel W. Lytle, and Edward A. Stern, J. Non-Cryst. Solids **8-10**, 401 (1972).
[24] Fredric J. Harris, Proc. IEEE **66**, 51 (1978).
[25] S. Sugai, Phys. Rev. B **35**, 1345 (1987).
[26] P. N. Sen and M. F. Thorpe, Phys. Rev. B **15**, 4030 (1977).
[27] David Chandler, *Introduction to Modern Statistical Mechanics* (Oxford University Press, New York, 1987), pp. 246–252.
[28] Marc Kastner, Phys. Rev. Lett. **28**, 355 (1972).
[29] Marc Kastner, David Adler, and H. Fritzsche, Phys. Rev. Lett. **37**, 1504 (1976).
[30] R. A. Street and N. F. Mott, Phys. Rev. Lett. **35**, 1293 (1975).
[31] K. M. Kandil *et al.*, Phys. Rev. B **51**, 17 565 (1995).
[32] R. W. Haisty and H. Krebs, J. Non-Cryst. Solids **1**, 399 (1969).
[33] R. A. Street, R. J. Nemanich, and G. A. N. Connell, Phys. Rev. B **18**, 6915 (1978).
[34] R. J. Nemanich *et al.*, Phys. Rev. B **18**, 6900 (1978).
[35] P. Eisenberger and S. Suckewer, Science **274**, 201 (1996).
[36] R. W. Schoenlein *et al.*, Science **274**, 236 (1996).